Global surface eddy diffusivities derived from satellite altimetry

R. P. Abernathey[1,2] and J. Marshall[1]

Received 30 May 2012; revised 11 December 2012; accepted 13 December 2012; published 25 February 2013.

[1] Velocities derived from AVISO sea-surface height observations, adjusted to be nondivergent, are used to simulate the evolution of passive tracers at the ocean surface. Eddy mixing rates are derived from the tracer fields in two ways. First, the method of Nakamura is applied to a sector in the East Pacific. Second, the Osborn-Cox diffusivity is calculated globally to yield estimates of diffusivity in two dimensions. The results from the East Pacific show weak meridional mixing at the surface in the Southern Ocean ($<1000\,m^2\,s^{-1}$, consistent with previous results) but higher mixing rates ($\sim$3000–5000 $m^2\,s^{-1}$) in the tropical ocean. The Osborn-Cox diagnostic provides a global picture of mixing rates and agrees reasonably well with the results from the East Pacific. It also shows extremely high mixing rates ($\sim10^4\,m^2\,s^{-1}$) in western boundary current regions. The Osborn-Cox diffusivity is sensitive to the tracer initialization, which we attribute to the presence of anisotropic mixing processes. The mixing rates are strongly influenced by the presence of a mean flow nearly everywhere, as shown by comparison with an eddy-only calculation, with the mean flow absent. Finally, results are compared with other recent estimates of mixing rates using Lagrangian and inverse methods.

Citation: Abernathey, R. P., and J. Marshall (2013), Global surface eddy diffusivities derived from satellite altimetry, *J. Geophys. Res. Oceans*, *118*, 901–916, doi:10.1002/jgrc.20066.

1. Introduction

[2] A large amount of the ocean's kinetic energy resides at the mesoscale in the form of geostrophic eddies, produced by the ubiquitous baroclinic instability of the large-scale density field [*Gill et al*., 1974; *Wunsch and Ferrari*, 2004]. These mesoscale eddies stir, mix, and transport tracers such as heat, salt, and potential vorticity, with significant consequences for the large-scale circulation and the climate system. The goal of this paper is to quantify and map eddy mixing rates globally. We accomplish this by simulating the evolution of passive tracers driven using satellite-derived surface geostrophic velocities and quantifying the mixing that ensues.

[3] The use of altimetric observations to infer mesoscale mixing rates is a problem with a substantial history [e.g. *Holloway*, 1986; *Keffer and Holloway*, 1988; *Stammer*, 1998]. The passive-tracer-based approach has recently been applied very successfully in a Southern Ocean context [*Marshall et al*., 2006; *Ferrari and Nikurashin*, 2010; *Shuckburgh et al*., 2009a, 2009b; *Abernathey et al*., 2010; *Klocker et al*., 2012b, 2012a]. These studies, like ours, simulated the advection of a passive tracer and then used the resulting tracer distributions to calculate "effective diffusivity" [*Nakamura*, 1996; *Winters and D'Asaro*, 1996]. Effective diffusivity directly measures the enhancement of mixing due to the stretching of tracer contours by eddies. An advantage of this method is that, in the limit of large Péclet number, and if the model resolution is sufficient to resolve the fine structure of tracer filaments (a.k.a. the Batchelor scale, which is set by an explicit small-scale diffusivity), the resulting diffusivities are independent of any unknown tuning parameters, including the small-scale diffusivity itself [*Shuckburgh and Haynes*, 2003; *Marshall et al*., 2006]. A disadvantage of the effective diffusivity method is that it produces only contour-averaged diffusivities, rather than two-dimensional maps.

[4] The effective diffusivity method has thus far only been applied to the Southern Ocean, for two apparent reasons: (1) eddy fluxes are known to be important there [*Johnson and Bryden*, 1989; *de Szoeke and Levine*, 1981], and (2), the geometry of the flow is well suited to the method. The diffusivity produced by the Nakamura method characterizes *cross-gradient* mixing as a function of tracer concentration. This information is most useful when the tracer in question has a clear monotonic gradient in the direction of interest. The strong fronts in the Southern Ocean have clearly defined consistent meridional gradients in density, temperature, and salinity [*Orsi et al*., 1995]. The mean flow of the ACC is aligned with these fronts, making the meridional tracer gradient easy to maintain for any weakly forced tracer. Thus, the mixing rates inferred from the effective diffusivity technique are readily interpreted as *meridional* diffusivities as a function of latitude [*Marshall et al*., 2006; *Abernathey et al*., 2010; *Ferrari and Nikurashin*, 2010].

[5] Our aim in this study is to use satellite-derived velocities and tracer-based methods to estimate mixing rates *globally*, not just in the Southern Ocean. As the first step

[1]Department of Earth, Atmospheric, and Planetary Science, Massachusetts Institute of Technology, Cambridge, Massachusetts, USA.
[2]Scripps Institution of Oceanography, La Jolla, California, USA.

Corresponding author: R. P. Abernathey, Scripps Institution of Oceanography, 9500 Gilman Drive #0213, La Jolla, CA 92093-0213, USA. (rabernathey@ucsd.edu)

2169-9275/13/10.1002/jgrc.20066

towards this end, we first examine a simplified version of the East Pacific, in which the mean flow is modified to be completely zonal and the domain is made zonally periodic, as in a channel. This allows us to compute effective diffusivity as a function of latitude using the same methods as *Marshall et al*. [2006], providing a useful starting point and connection to previous studies. We show that the mean flow has a strong role in shaping the mixing rates at all latitudes, not just in the Southern Ocean.

[6] To characterize mixing rates of the full flow, we turn to a different diagnostic: the *Osborn and Cox* [1972] diffusivity [see also *Nakamura*, 2001, 2008; *Lu and Speer*, 2010]. This diagnostic provides information about the local rate of irreversible mixing based on the tracer variance budget. Unlike effective diffusivity, which is based on a Lagrangian coordinate system, the Osborn-Cox diffusivity is Eulerian and can be applied in two dimensions. The Osborn-Cox diffusivity shows regions of strong mixing in the equatorial and western boundary current regions, with magnitudes exceeding $10^4\,\mathrm{m^2\,s^{-1}}$. Much weaker mixing of $O(500\,\mathrm{m^2\,s^{-1}})$ is found in the subpolar gyre regions. By performing the experiments with the mean flow removed, we also show that the mean flow does indeed play an important role in setting mixing rates in many regions of the global ocean.

[7] The paper is organized as follows. Section 2 describes the satellite data and tracer-transport model used in our study. In section 3, we present the effective diffusivity results from the East Pacific experiment. Section 4 introduces the Osborn-Cox diffusivity and describes the global experiments. In section 5, we conclude with a discussion of the results and a comparison with Lagrangian methods. Several appendices contain details of the methods and background theory.

2. Data and Numerical Advection Model

2.1. AVISO Geostrophic Velocity Data

[8] The satellite data used in this study are from the AVISO archive. Specifically, we use the geostrophic velocities derived from the gridded, delayed-time, reference, merged sea-level anomaly fields (known as *dt_ref_global_merged_msla_uv* in AVISO nomenclature.) We choose to use the precomputed geostrophic velocities, rather than computing our own from the sea-level anomaly for two reasons: (1) to facilitate easy replication of our results and (2) to take advantage of the sophisticated treatment employed by AVISO in computing velocities near the equator. The velocity fields are available on a 1/3° Mercator grid every 7 days. We use 17 years worth of observations, beginning with January 6, 1993.

[9] This data product resolves mesoscale eddies with radii of roughly 50 km and greater, which is below the dominant eddy length scale everywhere in the ocean [*Chelton et al*., 2011]. Nevertheless, there are certainly eddies smaller than 50 km present in the ocean, particularly at the submesoscales. How do these missing scales affect our calculations? As first noted by *Richardson* [1926], eddy diffusion in geophysical flows is itself a function of the length scale in question. Below the scale of the largest eddies, the diffusivity is determined either by local (in wavenumber space) or nonlocal dynamics, depending on the slope of the eddy kinetic energy spectrum *Bennet* [1984]. It is an active matter of research and debate whether particle dispersion and eddy diffusion at the mesoscales and submesoscales are local or nonlocal [*LaCasce and Ohlmann*, 2003; *Koszalka et al*., 2009; *Lumpkin and Elipot*, 2010]. But *above* the scale of the largest eddies, mixing becomes scale independent and is determined by the large-eddy dynamics. Our tracer-based diagnostics equilibrate on timescales of order of several months to a year, roughly corresponding to Lagrangian particle separations distances of greater than 200 km. At these large space and time scales, it is the well-resolved large eddies that determine the mixing rates. The smaller-scale mixing processes present at the submesoscales are in-effect parameterized by the grid-scale numerical diffusion included in our model. Therefore, our diagnosed diffusivities should be interpreted as corresponding to the large scales (>200 km) and not applicable to smaller-scale phenomena.

[10] The altimeter measures the anomaly of sea-surface height (SSH), which we will call h', from its mean height, and thus captures mesoscale variability. The geostrophic velocities associated with the SSH anomalies are

$$u'_{\mathrm{AV}}, v'_{\mathrm{AV}} = \frac{g}{f}\left(-\frac{\partial h'}{\partial y}, \frac{\partial h'}{\partial x}\right) \tag{1}$$

where $g = 9.8\,\mathrm{m^2\,s^{-1}}$ and f is the local Coriolis parameter (we use Cartesian coordinates here for notational simplicity, but in practice, all derivatives are computed appropriately for spherical geometry.) Geostrophic balance does not hold at the equator, but the altimetry data can still be used to infer velocities there, albeit with less confidence. The AVISO data set implements the method of *Lagerloef et al*. [1999] between ±5°. The basic balance underlying this method is the y-derivative of the meridional geostrophic balance at the equator: $\beta u' = -gh'_{yy}$ [*Picaut et al*., 1989]. The *Lagerloef et al*. [1999] method is essentially a way of matching this regime with the geostrophic regime away from the equator. The method has been validated with drifter data and has been demonstrated to capture the major features and variability of the equatorial circulation. Regardless, we must maintain some skepticism of our results near the equator.

[11] To conserve tracer under two-dimensional advection, the advecting velocity fields must be nondivergent and must have no flow normal to the boundary. The AVISO velocity fields must be modified to satisfy these conditions [*Marshall et al*., 2006]. The details of the numerical grid and the correction step are described in section A. The modification is generally very small relative to the flow itself. The corrected velocity fields are simply referred to as $v' = (u', v')$ henceforth.

2.2. Mean Flow

[12] The presence of mean flows can fundamentally alter mixing rates, and quantifying this effect on a global scale is a central goal of our study. Satellite altimetry most accurately measures only sea-level *anomaly*, not absolute sea-level, and therefore does not provide information about the mean flow. The best possible estimates of long-term mean flows are produced by ocean state estimation, in which all available observations, including those from the satellites in the AVISO archive, are assimilated in a physically consistent manner via an ocean model [*Wunsch and Heimbach*, 2009]. We use the time-averaged flow at 10 m depth from the ECCO-GODAE v3.73 state estimate, on a

1° grid, to define our mean flow. The flow is already approximately nondivergent, to order Rossby number. To make it fully nondivergent, it was interpolated and corrected in the manner described above for the AVISO data. Experiments are performed both with and without the mean flow. We use an overbar to denote the mean flow, such that the full velocity is given by $v(x,y,t) = \bar{v}(x,y) + v'(x,y,t)$.

[13] The AVISO archive also provides an "absolute dynamic topography" product that includes a mean flow at the surface. This mean flow product is referred to as *CNES-CLS09_v1*. We performed experiments using this mean flow and found minimal differences in results. The AVISO mean flow, on a 1/3° grid, contains narrower jets and other finer-scale features but does not differ greatly from the ECCO mean flow. Since the AVISO mean flow is also derived using data assimilation techniques, rather than "directly" observed, we prefer to use the ECCO product, which is calculated in such a way that it is guaranteed to be an optimal fit to the observations.

2.3. Advection/Diffusion Model

[14] To perform the tracer advection, we make use of the MITgcm framework [*Marshall et al*., 1997a, 1997b]. We employ the model in "offline" mode, where the dynamical core is disabled and the velocity fields are loaded from the AVISO data. The code simply solves the two-dimensional advection diffusion equation

$$\frac{\partial q}{\partial t} + v \cdot \nabla q = \kappa \nabla^2 q \tag{2}$$

where κ is a horizontal diffusivity and q is a passive tracer. Many different numerical schemes exist for solving this equation; we experimented with the standard second-order centered difference scheme and also a second-order scheme with a superbee flux limiter [*Roe*, 1985; *Hill et al*., 2012]. Both schemes performed reasonably. However, the second-order scheme without limiter sometimes introduced spurious extreme values of q, far outside its expected range, in regions of high mixing. These extreme values result in inflated ∇q, which corrupts the mixing diagnostics. For this reason, we opted to use the flux-limiting scheme. The tradeoff is that the flux limiter induces some amount of spurious numerical diffusion at the grid scale, in addition to the prescribed diffusion. This numerical diffusion is diagnosed and accounted for, following *Marshall et al*. [2006], using the methods described in section A.

3. Effective Diffusivity in a Pacific Sector

[15] Effective diffusivity developed as a diagnostic in the atmosphere [*Nakamura*, 1996; *Nakamura and Ma*, 1997; *Haynes and Shuckburgh*, 2000a, 2000b] and was later applied to the Southern Ocean/ACC system [*Marshall et al*., 2006; *Shuckburgh et al*., 2009a, 2009b; *Abernathey et al*., 2010]. Both these environments share an important feature: tracers have a strong, monotonic gradient in latitude, with the mean flow oriented perpendicular to the tracer gradients. The geometry of the mean flow in other ocean basins, however, is much more complex, with gyres, western boundary currents, and equatorial jets all contributing to the circulation. Furthermore, surface tracers (temperature and salinity) are not simply aligned with streamlines globally, as they are in the ACC, chiefly because strong air-sea forcing and vertical advection often dominate over advection by the horizontal flow. These issues make it very challenging to select an initial tracer distribution with which to perform a truly global effective diffusivity calculation.

[16] As a bridge to understanding mixing rates globally, we performed the following experiment: we took a sector in the East Pacific (180°W–130°W longitude, full range in latitude) and turned it into a re-entrant channel. This sector is unique in that it contains very little land and that the EKE is relatively homogenous in longitude. The mean flow (from ECCO) was zonally averaged and made constant in longitude ($\bar{u} = \bar{u}(y)$), with $\bar{v} = 0$ (the meridional mean flow was already weak in this sector.) The eddy velocities were derived from AVISO as described in the previous section and were made consistent at the overlap longitude during the correction step described in section 2.1 and section A. *Shuckburgh et al*. [2009b] and *Ferrari and Nikurashin* [2010] also performed experiments of this type in limited Southern Ocean sectors. Although this synthetic flow seems far removed from the real ocean, it contains the essential elements necessary to assess *meridional* mesoscale mixing rates in this sector.

3.1. Effective Diffusivity Calculation

[17] The effective diffusivity diagnostic measures the rate of material transport across tracer contours [*Nakamura*, 1996]. This transport is related to the length of the contour itself, with complex, highly filamented contours associated with higher effective diffusivity. Because its coordinate system follows the tracer, rather than being fixed in space, effective diffusivity is especially successful at identifying barriers to transport. Formally, the effective diffusivity is defined as

$$K_{\text{eff}} = \kappa \frac{L_e^2}{L_{\text{min}}^2}. \tag{3}$$

L_e is the "equivalent length" of a tracer contour deformed by eddies, L_{min} is the minimum possible contour length, and κ is the small-scale background diffusivity. The equivalent length of a tracer contour q, enclosing an area of $A(q)$, can be expressed as

$$L_e^2(q) = \frac{\frac{d}{dA}\int_A |\nabla q|^2 dA}{\left(\frac{\partial q}{\partial A}\right)^2} \tag{4}$$

where the integral is taken over the area A. This expression is easy to evaluate numerically for any instantaneous tracer concentration $q(x,y)$, and its value is readily mapped to an "equivalent latitude," i.e., the latitude of the mean tracer contour $\bar{q}(y)$ (a unique mapping between q and y is only possible if the meridional gradient of $\bar{q}$ is monotonic; this was part of the motivation to perform the simple periodic-domain experiment in the first place). Likewise, $L_{\text{min}}(y)$ is trivially defined as the width of the 50° domain at each point n latitude. Our initial tracer is proportional to latitude: $q(x,y,t=0) = y$.

[18] Once the calculation is initialized, the tracer quickly (within 2 or 3 months) forms fine structure due to eddy stirring, and L_e increases rapidly over this period. In the long

term, L_e is expected to decay as small-scale diffusion homogenizes the tracer; however, no strong decrease is observed over a 2-year period. Instead, L_e reaches a stable profile which evolves slowly due to seasonal and interannual variability of the eddy field. Other studies have found similar temporal behavior [*Marshall et al*., 2006; *Shuckburgh et al*., 2009a]. To compute a long-term mean value, we allow the tracer to evolve for a year and calculate L_e every month. At the end of the year, the tracer is re-initialized, and the process is repeated every year from 1993 to the end of 2009. A second tracer is also modeled, 6 months out of phase with the first. We compute a mean K_{eff} by averaging over the last 6 months of each tracer year. This mean value and its standard deviation (suggesting the interannual variability) are plotted in Figure 1b. As discussed in *Marshall et al*. [2006] and *Abernathey et al*. [2010], K_{eff} is almost completely independent of the choice of κ (we have confirmed explicitly that this is the case using experiments with different κ).

3.2. Discussion of Mixing Rates and Mean Flow Effects

[19] Building on work by *Taylor* [1921], *Prandtl* [1925], and *Keffer and Holloway* [1988], *Ferrari and Nikurashin* [2010] developed a simple analytical model for mixing across a jet, representing eddy effects with a stochastic advection term [see also *Klocker et al*., 2012a]. The cross-jet diffusivity was found to be

$$K_{\text{FN}} = \frac{\gamma}{\gamma^2 + k^2(\bar{u} - c)^2}\,\text{EKE} \tag{5}$$

where γ is the eddy decorrelation timescale, k the eddy wavenumber, $\text{EKE} = u'^2 + \bar{v}'^2/2$ the eddy kinetic energy, $\bar{u}$ the zonal mean flow, and c the eddy phase speed. A similar expression can be derived for the QGPV diffusivity in a baroclinically unstable flow [*Green*, 1970] and was used by *Smith and Marshall* [2009] and *Abernathey et al*. [2010] to interpret spatial patterns of diffusivity in the ACC. Here, we do not attempt to fit this formula to our results exactly; the parameters k, γ, and c can be difficult to assess, as documented in *Klocker et al*. [2012a]. Nevertheless, the formula provides a very useful framework for interpreting our diagnosed diffusivities. In particular, we see that K_{FN} depends not only on the eddy kinetic energy but also on the steering-level factor $(\bar{u} - c)^2$: given a particular EKE, the diffusivity is maximized when this term is zero, which corresponds to isotropic turbulence. The diffusivity can be suppressed by the propagation of eddies relative to the mean flow.

[20] To explore the influence of these factors, we plot v_{rms} (square root of EKE) and $\bar{u}$ for our domain in Figure 1a. We also plot an estimate of phase speeds c from the region inferred by Radon transforms of SSH data, courtesy of Chris Hughes (personal communication). The phase speed c is negative throughout most of the domain, consistent with the well-known westward propagation of eddies and Rossby waves [*Chelton and Schlax*, 1996; *Tulloch et al*., 2009]. To further probe the role of the mean flow, we also performed performed the same experiment with the *mean flow removed*, i.e., $\bar{u} = 0$. The K_{eff} for the zero mean flow case is shown as the dashed line in Figure 1b. In terms of (5), this experiment can be interpreted as replacing the suppression factor $(\bar{u} - c)^2$ with c^2 (it is important to remember that, in our kinematic model, removing the mean flow does not alter the phase speed c). According to the formula, in cases where $(\bar{u} - c)^2 > c^2$, setting $\bar{u} = 0$ results in higher K_{FN}; we refer to this as *mean flow suppression*. In cases where $(\bar{u} - c)^2 < c^2$, setting $\bar{u} = 0$ results in *lower* K_{FN}; we refer to this as *mean flow enhancement*. However, we reemphasize the point of *Ferrari and Nikurashin* [2010] that, by altering the mean flow, we are really just modulating the suppression factor in the denominator of (5). In no case does the presence of a mean flow truly enhance cross-jet mixing beyond the diffusivity expected for homogenous, isotropic turbulence. This should be kept in mind whenever we refer to mean flow "enhancement" in subsequent discussions.

[21] Beginning in the Southern Ocean, we see a picture already familiar from the work of *Marshall et al*. [2006], *Ferrari and Nikurashin* [2010], and *Klocker et al*. [2012a, 2012b]: relatively weak mixing in the core of the ACC where the mean flow is strongest (near 55°S) and slightly elevated values on the equatorward flank (north of 50°S) where eddy energy is still high but the mean flow is weaker. Comparing with the zero mean flow values, we see that the mean flow strongly suppresses mixing rates; without it, they reach values $>4000\ \text{m}^2\ \text{s}^{-1}$ in the ACC. Moving north to the midlatitudes, we see relatively uniform mixing between 40°S and 20°S of approximately $1000\ \text{m}^2\ \text{s}^{-1}$. It is intriguing to note, however, that the relatively weak eastward mean flow

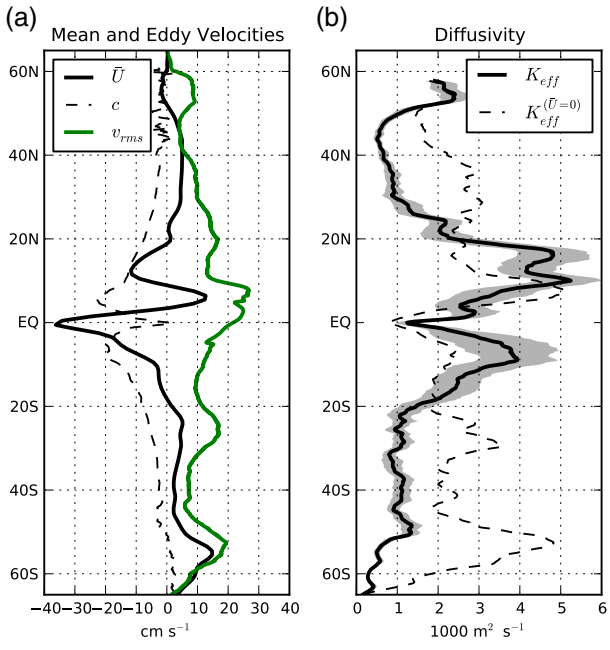

Figure 1. (a) Zonal mean flow $\bar{u}$, dominant phase speed c, and RMS eddy speed from the Pacific zonal sector experiment. The phase speed was diagnosed from the altimetric sea-surface height using Radon transforms by Chris Hughes (personal communication). (b) Diffusivity diagnostics. The mean K_{eff} is in black, with ±1 standard deviation in gray. The dashed line shows the mean K_{eff} produced when the mean flow is set to zero.

in this region still exerts a suppressing effect; without it, the mixing rates double.

[22] Moving further northward, a crucial transition occurs near 20°S. Here, observe a switch from mean flow suppression at high latitudes to mean flow enhancement at lower latitudes. This is also the latitude where the mean flow itself switches signs, from positive (eastward) to negative (westward). This behavior can be easily explained in terms of (5): south of this transition latitude, the phase speed c and mean flow $\bar{u}$ have the opposite sign, but north of it, they have the same sign. So south of the transition latitude, $(\bar{u}-c)^2 > c^2$, while north of it, $(\bar{u}-c)^2 < c^2$ (this concept is illustrated visually in Figure 1).

[23] The equatorial Pacific contains three distinct currents: the South Equatorial Current (westward), the Equatorial Counter Current (eastward, centered on 5°N), and the North Equatorial Current (westward, near 15°N). Consistent with (5), we observe mean flow enhancement in the South and North Equatorial currents, because $\bar{u}$ and c have the same sign there. But in the Counter Current, we have suppression because $\bar{u}$ is eastward while c is westward. Of course, the mixing rates are also modulated by the variations in EKE, but this experiment suggests a very strong role for the $(\bar{u}-c)^2$ term in equatorial region.

[24] In the rest of the North Pacific north of 20°N, the mean flow remains eastward and exerts a suppressing effect. The peak in K_{eff} near 55°N is associated with high EKE near the Aleutian islands and Alaskan coast.

[25] Overall, this sector displays a wide range of mixing rates, spanning an order of magnitude from 500 to 5000 $\text{m}^2\,\text{s}^{-1}$. These mixing rates are shaped by meridional variations in EKE, $\bar{u}$, and c. Especially high mixing rates in the subequatorial regions arise due to relatively high EKE combined with an alignment between the westward mean flow and westward propagating eddies.

4. Global Osborn-Cox Diffusivity

[26] The East Pacific is ideal for investigating mixing rates using K_{eff} because of its lack of land and relative zonal symmetry. But focusing only on this sector neglects the most energetic regions of the global ocean: the western boundary currents. The complicated flow geometry near western boundaries makes it problematic to calculate K_{eff} there, because the mapping between tracer contours and a physical location in space breaks down. More generally, it is desirable to quantify tracer mixing rates in two dimensions, which will never be possible using the effective diffusivity method.

4.1. Definition

[27] In order to quantify mixing locally, we must employ a suitable definition. From a Lagrangian standpoint, mixing means the decorrelation of particle trajectories; the "mixing rate" is proportional to the rate of decorrelation. A key property of this process is its irreversibility, through which particles "forget" where they came from. For tracers, mixing means the generation of small length scales which, in the presence of small-scale diffusion, leads to irreversible homogenization of tracer concentration [*Ottino*, 1989; *Nakamura*, 2008]. This is precisely what is measured by effective diffusivity. The Osborn-Cox diffusivity is a diagnostic which attempts to quantify this process *locally* [*Osborn and Cox*, 1972]. Since mixing is not, in fact, a local process, this objective is inherently problematic. Nevertheless, it is informative to separate the local, irreversible mixing from the eddy transport due to other, reversible processes [*Marshall and Shutts*, 1981; *Nakamura*, 2001]. Furthermore, since our experiments show that mixing is approximately local on large scales, the Osborn-Cox diffusivity can be regarded as a reasonable approximation to the overall eddy diffusivity.

[28] The origin of the Osborn-Cox diffusivity is in the tracer variance budget. We briefly review its derivation here, following *Nakamura* [2001], to clarify its physical interpretation. By taking a time mean of (2), we obtain the Reynolds-averaged tracer equation:

$$\frac{\partial \bar{q}}{\partial t} + \bar{v}\cdot\nabla\bar{q} = -\nabla\cdot\overline{v'q'} + \kappa\nabla^2\bar{q}. \tag{6}$$

[29] The overbar indicates a time/ensemble mean and a prime a departure from that mean, such that $q = \bar{q} + q'$. This equation describes the evolution of the mean tracer $\bar{q}$ and looks identical to (2) except for the eddy flux term on the right. The general eddy parameterization problem is often framed in terms of determining a tensor $\mathbf{K}$ that relates the eddy flux term in (6) to the mean background gradient, such that $\nabla\cdot\overline{v'q'} = \nabla\cdot(-\mathbf{K}\nabla\bar{q})$ [*Plumb and Mahlman*, 1987; *Griffies*, 1998]. Many processes besides mixing can contribute to $\mathbf{K}$, including eddy-induced advection, reversible displacement of tracer contours, and advection of tracer variance. Our goal here is not to determine $\mathbf{K}$ fully but rather to isolate, map, and quantify the irreversible mixing which arises due to stirring by eddies.

[30] Mixing is associated only with eddy fluxes that are down the mean gradient. To highlight this portion of the flux, (6) can be uniquely rearranged to the form

$$\frac{\partial \bar{q}}{\partial t} + (\bar{\boldsymbol{v}} + \boldsymbol{v}^*)\cdot\nabla\bar{q} = \nabla\cdot[(K+\kappa)\nabla\bar{q}] \tag{7}$$

where v^* is an eddy-induced advection (formed from the antisymmetric part of $\mathbf{K}$) and K is a scalar eddy diffusivity for the eddy flux in the direction normal to the mean gradient, defined such that $-K\nabla\bar{q} = \overline{v'q'}\cdot\nabla\bar{q}/|\nabla\bar{q}|$. The tracer variance budget constrains the sign and magnitude of K. The variance budget is obtained by subtracting (6) from (2), multiplying by q' and taking the average. The resulting equation is

$$\frac{\partial}{\partial t}\frac{\overline{q'^2}}{2} + \nabla\cdot\overline{v\frac{q'^2}{2}} + \overline{v'q'}\cdot\nabla\bar{q} = \nabla^2\left(\kappa\frac{\overline{q'^2}}{2}\right) - \kappa\overline{|\nabla q'|^2} \tag{8}$$

where the quantity $\overline{q'^2}/2$ is the tracer variance. Substituting the definition of K into the last term on the LHS, we can solve for K to find

$$K = K_K + K_{\text{OC}} \tag{9}$$

where

$$K_K = \left[\frac{\partial\overline{q'^2}}{\partial t} + \nabla\cdot\left(\overline{vq'^2} - \kappa\nabla\overline{q'^2}\right)\right]/2|\nabla\bar{q}|^2 \tag{10}$$

and

$$K_{\mathrm{OC}} = \kappa \frac{\overline{|\nabla q'|^2}}{\overline{|\nabla q|^2}} \tag{11}$$

[31] K_K arises due to time evolution in the variance field or from the transport of variance. The tendency term is generally small in our simulations, except in a few particular locations (discussed subsequently). The variance advection term includes both mean advection $\bar{v}\overline{q'^2}$ (related to the "rotational flux" discussed by *Marshall and Shutts* [1981]) and the triple correlation term $\overline{v'q'^2}$. These terms are zero in isotropic, homogeneous turbulence, and regardless of the details of the turbulence, they vanish in a globally integrated budget. Locally, they can be either positive or negative [*Wilson and Williams*, 2004]. Detailed diagnostics of the terms in the variance budget are performed in section C.

[32] The Osborn-Cox diffusivity K_{OC} is a diffusivity for the part of the downgradient eddy flux associated with irreversible mixing. The physical interpretation of K_{OC} resembles that of K_{eff}: it quantifies the enhancement of small-scale diffusion due to fine-scale tracer gradients created by eddy stirring. The factor $\overline{|\nabla q'|^2}/|\nabla \bar{q}|^2$ can be interpreted as ratio of length scales that measures the efficiency of this process, just like the factor L_e^2/L_{min}^2 in K_{eff}. In fact, it can be shown that K_{OC} integrated along a tracer contour is equivalent to K_{eff} [see *Nakamura*, 1996, equation 2.2–2.5]. But because K_{OC} is a positive-definite Eulerian mean quantity, it can be used to produce a two-dimensional map of mixing rates.

4.2. Experiments

[33] The methodology we use for the global experiments follows in a straightforward way from the previous section. We initialize a tracer globally, stir it with the corrected AVISO velocity field v' in combination with the ECCO mean flow $\bar{u}$, and reset the tracer after 1 year. The process is repeated for 17 years of AVISO data; the statistics necessary to compute K_{OC} and the terms of the variance budget are generated by time averaging over the whole 17-year period. This procedure can be viewed as an ensemble of 17 individual yearly experiments. The results are not very sensitive to the averaging period, provided the period is short enough to prevent the tracer gradients from being completely mixed away; in which case, K_{OC} becomes undefined.

[34] A central challenge in designing the global experiment is the choice of an initial tracer, which we call $q_0 = q(x, y, t = 0)$. The above derivation makes it clear that K_{OC} should be interpreted as a diffusivity *across* the mean gradient $\nabla \bar{q}$. Therefore, although K_{OC} is a scalar quantity, there is an implicit orientation to the mixing process it represents. The orientation of $\nabla \bar{q}$ is determined in part by q_0 and in part by the flow itself, which tends to work to align the tracer with the jets. Observations and simulations of drifter trajectories suggest that particle dispersion and tracer diffusivity in the ocean are highly anisotropic, with zonal or along-stream dispersion occurring much more rapidly than in the meridional/cross-stream direction [*Sallée et al*., 2008; *Kamenkovich et al*., 2009; *Griesel et al*., 2010; *Rypina et al*., 2012; *Fox-Kemper et al*., 2012] (the likely explanation for this anisotropy is the mechanism of "shear dispersion" [*Young et al*., 1982], which describes how mixing is enhanced along the jet axis in the presence of a sheared mean flow). These considerations suggest that if the mean jet crosses the contours of q_0, higher values of K_{OC} will result. Our experiments confirm this hypothesis.

[35] Here, we describe the results of experiments with three different tracer initializations,

$$q_0 = \begin{cases} \varphi & \text{latitude } (\texttt{trLAT}) \\ \psi & \text{streamfunction for the mean flow } (\texttt{trPSI}) \\ \theta & \text{climatological sea} - \text{surface temperature } (\texttt{trSST}) \end{cases} \tag{12}$$

[36] The use of latitude as an initial tracer (an experiment we refer to as `trLAT`) is an obvious option. Its meridional gradient means that K_{OC} is associated with a meridional diffusivity, in clear analogy with the previous section. However, with `trLAT`, there is no consistent global relationship between the tracer and the ocean jets; contours of `trLAT` are more or less aligned with the ACC and the equatorial jets but are perpendicular to western boundary currents.

[37] An alternative possibility is to use an initial tracer that is perfectly aligned with the mean flow everywhere. The streamfunction ψ for the mean flow defines such a tracer. We call this experiment `trPSI`. The K_{OC} produced by this experiment can be interpreted as representative of cross-stream mixing. A major disadvantage of `trPSI` is that it contains local maxima and minima, for instance, in the middle of gyres or in the alternating jets of the equatorial Pacific. In our experiments, vanishingly weak background gradients $|\nabla \bar{q}|$ in these regions lead to spuriously high K_{OC} values. Such spurious values do not necessarily represent regions of strong mixing but rather are implicit in q_0. Furthermore, the local extrema tend to be mixed away quickly, which leads to significant time dependence in the variance budget, further undermining the validity of K_{OC} in these regions. We also explore the third tracer, the mean sea-surface temperature θ, which is somewhat aligned with the mean flow but contains different local extrema from `trPSI`.

4.3. Maps of K_{OC}

[38] The results for the three experiments are shown in Figure 2 on a logarithmic scale. Despite significant difference in the variance budgets themselves (see section C), all three calculations share the following key attributes in K_{OC}:

- Large values ($K_{\mathrm{OC}} > 10^4$ m^2 s^{-1}) on the flanks of western boundary currents such as the Gulf Stream and Kuroshio (though this is not necessarily a cross-stream diffusivity)
- Local minima ($K_{\mathrm{OC}} < 10^3$ m^2 s^{-1}) in the subpolar gyres around 45°N/S
- Patterns in the Southern Ocean consistent with *Marshall et al*. [2006], with high values on the northern flank of the ACC and lower values farther south
- Very high values in the tropics, but with somewhat differing spatial patterns

[39] Many of the apparent differences can be understood in terms of the issues reviewed above. Both `trLAT` and `trSST` exhibit high K_{OC} in the western boundary current

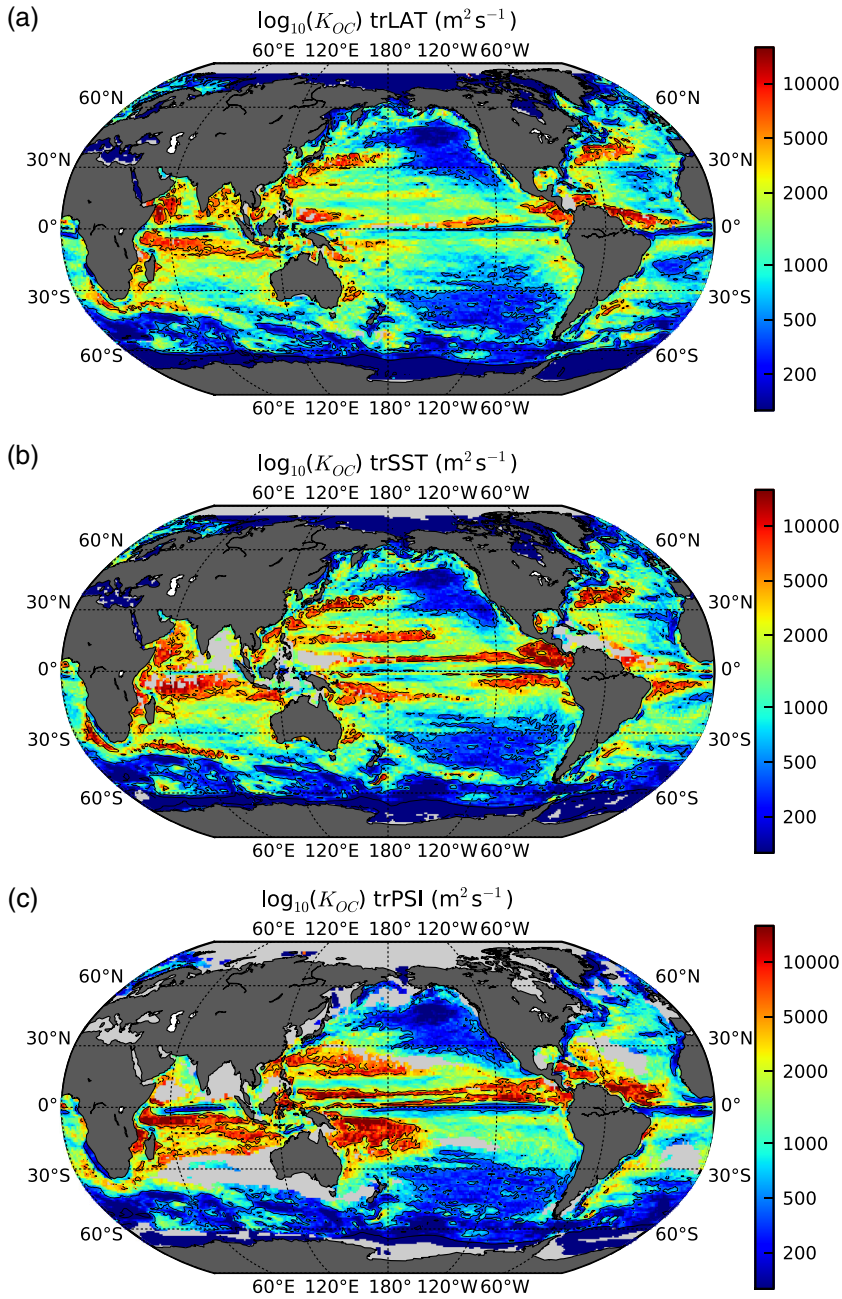

Figure 2. Osborn-Cox diffusivity on a logarithmic scale, i.e., $\log_{10}(K_{OC})$. The initial tracer concentrations used were (a) latitude, (b) SST, and (c) streamfunction for mean flow. The values have been masked in areas where $|\nabla\bar{q}|$ is very weak. Solid black contours are included at values of 1000 and 10,000 $m^2\,s^{-1}$.

extension regions. `trPSI`, on the other hand, does not have such a pronounced maximum in these regions. We attribute this to the fact that `trPSI` is totally aligned with the mean currents in these regions, while the others are not. The misalignment means that the tracers experience the much stronger along-stream mixing rate, rather than the weaker cross-stream mixing rate felt by `trPSI`. This conclusion is supported by the experiments with no mean flow, presented in the next section.

[40] As also mentioned above, K_{OC} becomes undefined where $|\nabla\bar{q}|^2 = 0$. `trLAT` avoids this situation better than the other tracers because it contains no pre-existing local extrema. For both `trSST` and `trPSI`, however, the q_0 field contains local maxima to begin with, and these points inevitably are associated with very large values of K_{OC}. Figure 2 masks the areas where $|\nabla\bar{q}|$ is less than equal to 10% of its global mean value, i.e., where the background gradients are very weak. There are almost no such areas for the latitude tracer, but there are several large regions for the other tracers. This mask, however, does not remove all the problems associated with the weak initial gradients. For instance, the banded structures in K_{OC} near the equator in the `trPSI` experiment are clearly due to the bands in the streamfunction itself, which arise due to the alternating

zonal jets in this region. trLAT, which has no such small-scale variations in its initial conditions, does not display these structures.

[41] Further discussion and interpretation of the results, and a comparison with other studies, can be found in section 5.

4.4. Impact of Mean Flows

[42] The role of the mean flow in determining the spatial pattern of K_{OC} can be assessed by conducting the global experiment with the mean flow set to zero. We call the Osborn-Cox diffusivity obtained this way $K_{OC}^{u=0}$. We show results of these experiments for trLAT and trPSI in Figures 3 and 4. As discussed above, these two tracers have very different orientations relative to the mean flow, in particular in the western boundary current regions, where trLAT is nearly perpendicular to the mean flow. trPSI, on the other hand, is always perfectly aligned with the mean flow. The effect of removing the mean flow will be different in each case. By removing the mean flow from the trLAT experiment, we eliminate the effects of shear dispersion along jet axes. Because trPSI does not experience these effects as strongly, that experiment provides a closer analogy with the zonally symmetric results of section 3, in which all mixing was by construction "cross front."

[43] Focusing first on trPSI (Figure 4), we note similar patterns of suppression and enhancement to those found in the Pacific channel experiment of section 3 (compare with Figure 1). We observe strong suppression by the mean flow throughout the ACC. In the tropics where the mean flows become westward (the same sense as Rossby wave propagation), the presence of the mean flow leads to enhancement which is correlated with the structure of the equatorial jets. Where the Equatorial Counter Current flows eastward, we observe suppression. In the western boundary currents and their extension jets that flow eastward between the subtropical and subpolar gyres, we observe significant suppression. Just as in the ACC, the combination of eastward flow and westward propagating waves/eddies leads to suppression of mixing. It has been suggested [*Bower et al.*, 1985] that the Gulf Stream creates a mixing barrier near the surface, and our results here are consistent with this interpretation.

[44] For the most part, the effects of the mean flow on trLAT are similar, with the same broad patterns of enhancement and suppression. There is a big difference, however, in the western boundary current regions. In the core of the Gulf Stream, and on the northern flank of the Kuroshio extension, the mean flows clearly suppress mixing, as observed across the region for trPSI. However, for trLAT, the addition of the mean flow causes extremely *enhanced* mixing on the southern flanks. We interpret this as mixing along the jet axis caused by shear dispersion, which is possible due to the initial misalignment between trLAT and the current.

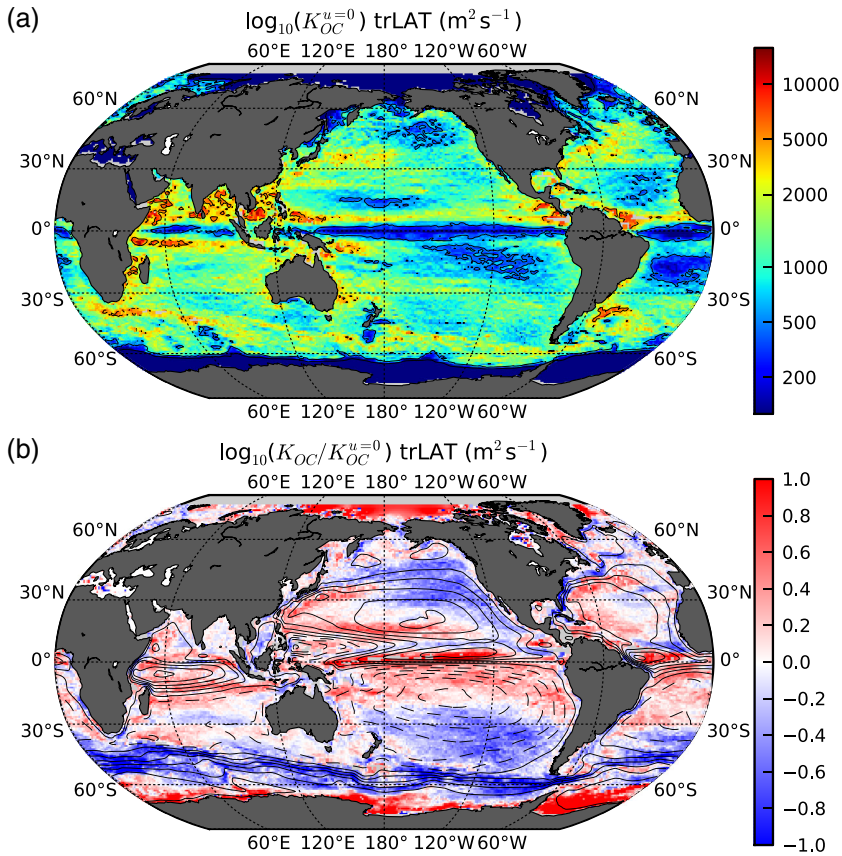

Figure 3. (a) Osborn-Cox diffusivity on a logarithmic scale for the latitude tracer experiment (trLAT) with the mean flow set to zero. (b) The log ratio between K_{OC} with and without the mean flow. The black contours are the streamfunction of the mean flow, indicating the position of mean currents.

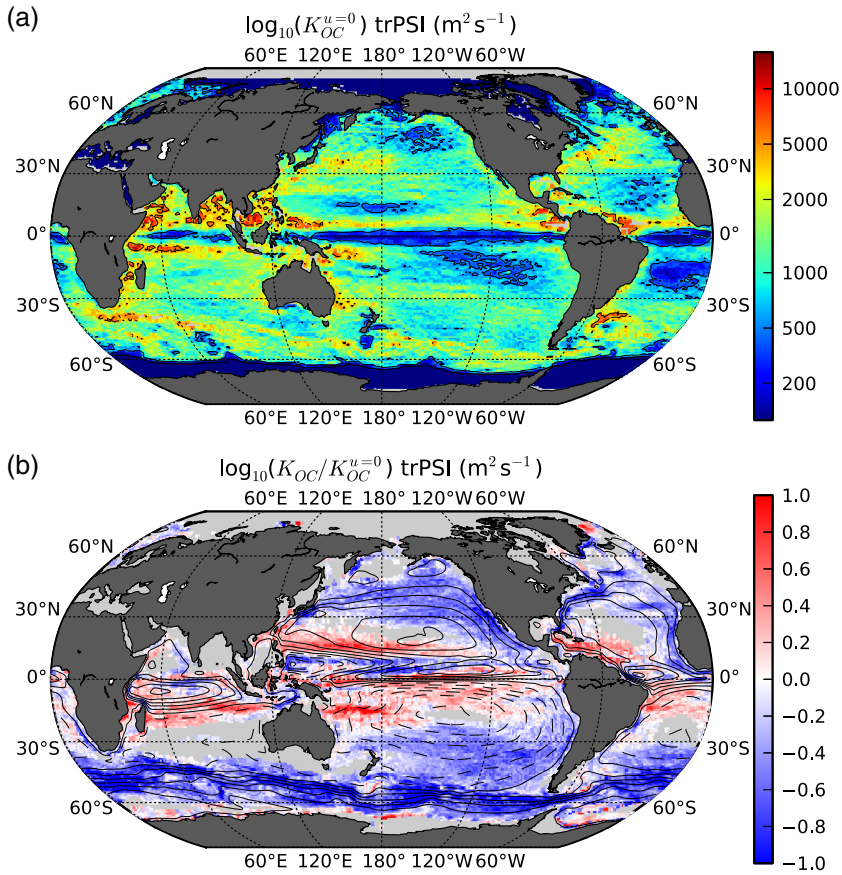

Figure 4. Same as Figure 3 but for `trPSI`.

[45] To gauge the potential effects of shear dispersion, we can employ the simple scaling derived by [*Young et al.*, 1982]. Their model predicts an enhanced downstream diffusivity of

$$K_\alpha = \kappa \frac{1}{2}\left(\frac{\alpha}{\omega}\right)^2 \tag{13}$$

where α is the mean flow shear and ω is the wave angular frequency. Typical values in a boundary current region such as the gulf stream are $\alpha \simeq 10^6$ s^{-1} and $\omega \simeq 10^8$ s^{-1}. This crude estimate indicates that shear dispersion is capable of producing diffusivities 5000 times the background diffusivity κ. This suggests that shear dispersion is indeed a plausible mechanism for producing the elevated downstream mixing in these regions.

5. Discussion and Conclusions

5.1. Summary

[46] We have constructed a global map of eddy mixing rates based by using satellite observations to simulate the evolution of passive tracers. We began in a "zonalized" version of the East Pacific, where we computed effective diffusivity as a function of latitude. We found surprisingly high mixing rates (>5000 m^2 s^{-1}) in the tropics. We saw that the zonal mean flow acts to suppress mixing at high latitudes, where the flow is eastward, as previous studies in the ACC have already confirmed. However, between 30°N and S, where the mean flow is westward, the presence of a mean flow actually *enhances* mixing rates. We suggested that this behavior arises due to the westward phase speed of eddies and waves. When the mean flow and the phase speed have the same sign, as in the westward-flowing equatorial currents, the mean flow enhances mixing. When they have the opposite sign, as in the eastward-flowing equatorial counter current or in most of the mid-latitude ocean, the mean flow suppresses mixing. Near the equator, where the mean flow consists of zonal jets of alternating sign, we saw complex patterns of enhancement and suppression.

[47] We then introduced the Osborn-Cox diffusivity K_{OC}, which arises from the tracer variance budget. We reviewed how K_{OC} captures the part of the cross-gradient eddy flux that is locally balanced by dissipation. When the variance budget is nonlocal and nonsteady, there are additional fluxes not captured by K_{OC} (in section C we show, both in the Pacific channel model and in global simulations, that these effects are generally small; the variance budget contains nonlocal fluxes on scales of O(500 km), but the overall balance between variance production and dissipation is captured well by K_{OC}).

[48] We calculated K_{OC} from global simulations using three different initial tracers: one aligned with latitude, one proportional to the streamfunction of the mean flow, and one proportional to SST. Despite significant differences in the variance budget for these tracers, the resulting K_{OC} values showed similar large-scale structure and magnitudes.

Differences arose in regions with weak initial background tracer gradient and in regions where the initial tracer was strongly perpendicular to the mean flow. We also performed global experiments with the mean flow set to zero—these confirmed the general picture of mean flow suppression at high latitudes and mean flow enhancement at low latitudes. The effect of the mean flow in the boundary current regions was much more tracer dependent.

5.2. Comparison With Other Studies

[49] Most studies of lateral mixing in the ocean are based on the statistics of particle dispersion [*Owens*, 1984; *Davis*, 1991; *LaCasce and Bower*, 2000; *Lumpkin et al*., 2002; *Zhurbas and Oh*, 2003; *Zhurbas and Oh*, 2004; *LaCasce*, 2008; *Waugh and Abraham*, 2008; *Sallée et al*., 2008; *Lumpkin and Elipot*, 2010; *Rypina et al*., 2012]. Such Lagrangian methods are particularly valuable because they can take advantage of the ample surface-drifter trajectory data. One limitation of these Lagrangian methods is that they are constrained by the number of particles within the area of interest, leading to a tradeoff between precision and spatial resolution. There are also challenges associated with translating Lagrangian particle statistics into the Eulerian eddy diffusivities required by numerical ocean models. *Klocker et al*. [2012b] recently showed that particle-based and tracer-based diffusivities agree well in a simple channel flow resembling a sector of the ACC, but it is unclear whether this result applies to the more complex flow geometries of the real ocean. In general, tracers and particles both provide valuable information and should be considered complimentary.

[50] The recent study by *Rypina et al*. [2012] is an important point of comparison for our results. These authors performed a comprehensive analysis of particle spreading and the associated Lagrangian diffusivities in the North Atlantic, focusing on the anisotropy of the spreading process and using both simulated and observed trajectories. They found that, at most locations, spreading is faster (and therefore diffusivity is greater) in the meridional direction. But in the Gulf Stream, they found that the fastest spreading occurs along the axis of the current, with slower spreading (and weaker diffusivity) across the stream. The magnitudes of along-stream mixing exceeded 10^5 m^2 s^{-1} in places, while the cross-stream mixing did not exceed 5000 m^2 s^{-1}. Our K_{OC} diagnostic, which is a scalar, cannot distinguish this anisotropy using a single tracer. However, the presence of anisotropic mixing seems clearly related to the differing values of K_{OC} we found from different tracers; the tracers with gradients perpendicular to the Gulf Stream experienced much stronger mixing. When this effect is taken into account, the magnitudes of diffusivity we found are totally compatible with *Rypina et al*. [2012], and the spatial patterns are also similar. Furthermore, *Rypina et al*. [2012] compared statistics from real drifters with simulated trajectories from the AVISO data set (the same one we have used) and concluded that, on large scales, there was strong qualitative agreement. The real drifters produced somewhat *higher* values of diffusivity than the simulated trajectories.

[51] As the comparison with *Rypina et al*. [2012] suggests, one limitation of our method based on K_{OC} is the representation of the mixing process as a scalar quantity. A more general definition of eddy diffusivity involves a tensor diffusivity which relates the eddy flux in each direction to each component of the gradient [*Plumb*, 1979; *Redi*, 1982; *Plumb and Mahlman*, 1987; *Griffies*, 1998]. The recent study by *Fox-Kemper et al*. [2012] attempts to grapple with the full three-dimensional diffusivity tensor, diagnosed from multiple passive tracers in an eddy-permitting numerical model. Their results, like those of *Rypina et al*. [2012], indicate strong anisotropy in mixing rates, with a large major-axis diffusivity (whose magnitude exceeds 6000 m^2 s^{-1} over large parts of the ocean) and a smaller minor-axis diffusivity. The ranges of values and spatial patterns they find are broadly consistent with our results as well. Their results, however, also show a significant degree of small-scale "noise" in the diffusivities, including negative values, pointing to a downside of that approach.

[52] A final important reference is the recent study by *Liu et al*. [2012], who used an adjoint-based inverse method to estimate eddy diffusivities within a coarse-resolution numerical model, producing 3-D maps of the *Gent and McWilliams* [1990] coefficient (K_{GM}), as well as other values relevant for eddy parameterization. Although the relationship between these quantities and the diagnostics described here is indirect, certain similarities emerge, such as elevated K_{GM} in parts of the western boundary regions. Direct comparison is hampered by the fact that K_{GM} and K_{OC} represent physically distinct processes and by the strong vertical variations in the estimates of *Liu et al*. [2012]. Furthermore, *Liu et al*. [2012] do not allow the mixing coefficients to be anisotropic, which could potentially explain their model's misfit in jet regions. The magnitudes of K_{GM} they find rarely exceed 2000 m^2 s^{-1}, but this is not necessarily in conflict with our findings. Overall, their study supports the notion that spatially variable eddy mixing is an important ingredient of ocean circulation.

5.3. Composite K_{min} From Multiple Tracers

[53] From the discussion above, we surmise that the different tracers experience different K_{OC} because of the inherent anisotropy in the mixing process. As a final step, we present a composite map showing the *minimum* value of K_{OC} from each experiment at each point in space in Figure 5 (we call this quantity K_{min}). It is our hope that such a map can be a useful guide for coarse-resolution ocean models to employ spatially variable mixing rates. Of course, an anisotropic tensor diffusivity would be more appropriate than a scalar in parameterizing the full complexity of eddy transport [*Redi*, 1982; *Griffies*, 1998; *Fox-Kemper et al*., 2012]. But in practice, many large-scale ocean models are quite far from this degree of sophistication. *Liu et al*. [2012] clearly demonstrate that a spatially variable yet isotropic diffusivity can lead to a significant improvement in model performance. K_{min} effectively defines a lower bound on the mixing rate. The rationale for suggesting K_{min} is that, especially in frontal regions, it is more important to accurately represent (and not overestimate) the across-stream mixing rather than the downstream mixing. This is because lateral mixing is often the only way for cross-frontal transport to occur, while downstream transport is easily accomplished by the jet itself.

[54] Besides the issue of anisotropy, another central challenge in applying our results to ocean models is the question of the vertical variation in mixing rates. The mixing rates presented here are derived from the surface geostrophic flow; they should be applicable over the surface mixed layer,

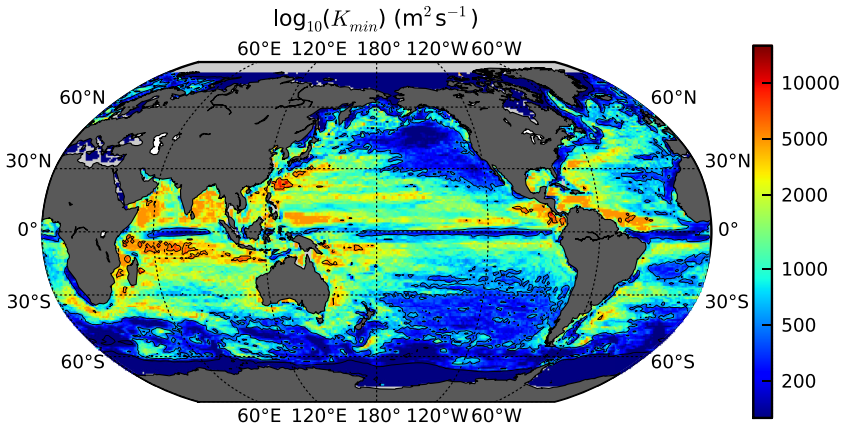

Figure 5. Composite value of K produced by taking the minimum K_{OC} at each point from the three experiments. See text for discussion.

in which there is no geostrophic shear. The issue of how to extrapolate altimetric observations to infer currents at depth is an extremely active topic of research at present, with no clear consensus on the best method [*Wunsch*, 1997; *Lapeyre*, 2009; *Scott and Furnival*, 2012]. Further complicating the picture is the fact that, although eddy kinetic energy generally decays with depth, the diffusivity itself can have pronounced mid-depth maxima when the mean flow suppression effects decay more quickly than the EKE [*Smith and Marshall*, 2009; *Abernathey et al*., 2010; *Klocker et al*., 2012a]. While those previous studies focused only on the Southern Ocean, we suspect that mid-depth mixing maxima are also present in the Northern Hemisphere western boundary currents and their extension jets. A deeper understanding of the vertical structure of eddy mixing globally is therefore a top priority for future research.

[55] Despite the many caveats, it is interesting to speculate about the implications of our results for the modeling of ocean general circulation. Conventional coarse-resolution ocean models usually employ a uniform eddy mixing rate of around 1000 $m^2\,s^{-1}$. Our results indicate that near-surface mixing rates are *at minimum* at three or four times this large in broad areas of the tropical ocean. This implies a much greater role for eddy-induced transport in these regions. Corroborating this conclusion is the comment by *Danabasoglu and McWilliams* [1995] that an enhanced eddy mixing coefficient in the tropical Pacific significantly reduced the misfit between their coarse model and the observations. On the other hand, it seems likely that eddy effects are *overestimated* by such models in large parts of the subpolar gyres, where mixing rates of 500 $m^2\,s^{-1}$ and less are prevalent. It is our hope that the estimates provided in this paper can serve as a useful observational reference point in the ongoing effort to improve the parameterization of mesoscale eddies in ocean and climate models.

Appendix A: Velocity Field Interpolation and Divergence Correction

[56] In order to resolve fine-scale filaments in the tracer field, we model the tracer advection at finer resolution than the original AVISO grid. The raw AVISO velocity fields are linearly interpolated to a 1/10° lat-lon grid. The boundaries for the fine resolution grid are derived from the GEBCO 1-arc-min gridded data, distributed by the British Oceanographic Data Service.

[57] To conserve tracer under two-dimensional advection, the advecting velocity fields must be nondivergent and must have no flow normal to the boundary. However, divergence is present in the AVISO-derived velocities for several reasons: (1) the variation of f with latitude, (2) the algorithm used at the equator, and (3) the interpolation to a finer grid. Furthermore, the normal flows are also not guaranteed to vanish at the boundaries. We therefore derive nondivergent velocities from the AVISO fields following the procedure of *Marshall et al*. [2006]. Via a Helmholtz decomposition, the full AVISO field can be written as the sum of a nondivergent stream function component and a velocity potential component:

$$v'_{AV} = \nabla \times \psi + \nabla\chi. \tag{A1}$$

[58] The "corrected," divergence-free field is

$$v' = v'_{AV} - \nabla\chi. \tag{A2}$$

[59] To determine χ, we solve the elliptic problem

$$\nabla \cdot v'_{AV} = \nabla^2\chi. \tag{A3}$$

subject to the boundary condition $\nabla\chi = v'_{AV} \cdot \hat{n}$ to eliminate flow normal to the boundary. Over most of the ocean, the correction term is $O(0.1)$ or less when compared to the eddy velocities. The ratio only exceeds 0.5 near boundaries in the equatorial region.

Appendix B: Numerical Diffusivity and Sensitivity of Results to κ

B1. Quantifying Numerical Diffusivity

[60] The small-scale diffusivity κ plays an important role in several mixing diagnostics. It is well known that numerical advection/diffusion can introduce extra diffusion beyond what is specified explicitly by κ. We quantify this

effect, as done in *Marshall et al*. [2006] and *Abernathey et al*. [2010], through the domain-averaged tracer variance budget. Multiplying (2) by q and taking an integral over the entire domain gives

$$\frac{\partial}{\partial t}\int\int\frac{q^2}{2}dA = -\kappa_{\mathrm{num}}\int\int|\nabla q|^2 dA \tag{B1}$$

where the quantity κ_{num} is a measure of the total amount of diffusion, explicit and implicit, in the model (by taking κ_{num} outside the integral, we have assumed that it, like the explicitly specified κ, is constant in space; this assumption may not be valid, but computing the numerical diffusivity locally is not possible with this method). We can evaluate these integrals from the model output and solve for κ_{num}. We tested values of κ ranging from 25 to 150 $\mathrm{m^2\ s^{-1}}$. Tracers were initialized with a gradient in latitude and evolved for 1 year, with q output every month. This was repeated for four separate years of altimetric data. The result indicates that κ_{num} is maximum at the beginning of the advection but within a few months settles into a reasonably steady state. The mean values of κ_{num} are given in Table B1. In what follows, κ_{num} will always be used in place of the raw κ when analyzing our simulations.

B2. K_{OC} Dependence on κ

[61] Here, we address the degree to which K_{OC} is independent of κ. The factor $\left|\nabla\bar{q}\right|^2$, the mean background gradient, is set primarily by the initial conditions and is independent of κ, so K_{OC} will be independent of κ if $\left|\nabla q'\right|^2 \propto \kappa^{-1}$. Employing the same set of experiments used to calculate κ_{num}, we calculated the domain-averaged value of $|\nabla\bar{q}'|^2$ for a range of κ. The results, shown in Figure B1 on a logarithmic scale, do indeed show that this factor is inversely proportional to κ, with power-law relationship close to -1. A linear fit of the points in Figure B1 reveals that, actually, $\left|\nabla q'\right|^2 o\kappa^{-0.8}$. The departure of the exponent from -1 means that K_{OC} does depend weakly on κ: specifically, that $K_{\mathrm{OC}} \propto \kappa^{-0.2}$.

[62] Measurements of the true background diffusivity in the ocean on scales of 1–10 km have been estimated by *Ledwell et al*. [1998] from deliberate tracer release experiments. Based on observations of tracer filament width, they concluded that $\kappa \simeq 2\ \mathrm{m^2\ s^{-1}}$ at 300 m depth in the North Atlantic. This is significantly less than the $\kappa_{\mathrm{num}} = 66\ \mathrm{m^2\ s^{-1}}$ value we used. Assuming the $\kappa^{-0.2}$ dependence holds down to such low values of κ, we can extrapolate what value of K_{OC} would result from to employing $\kappa \simeq 2\ \mathrm{m^2\ s^{-1}}$. Since

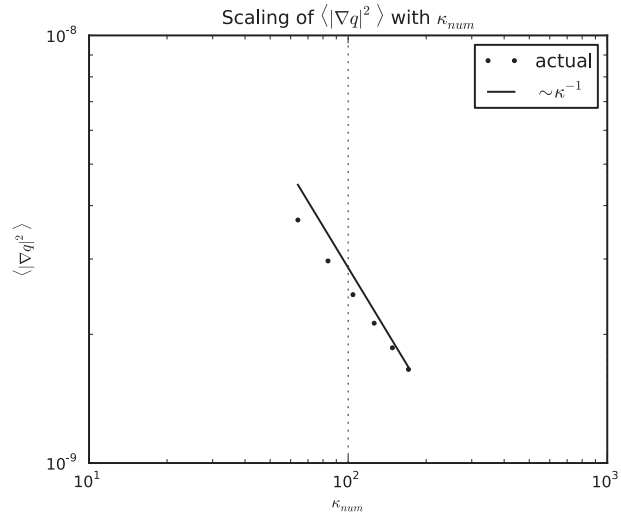

Figure B1. Relationship between κ_{num} and κ if $|\nabla\bar{q}'|^2$ diagnosed for six different values of κ. The solid line represents a -1 power-law dependence.

$(2/66)^{0.2} \simeq 0.50$, this implies that that our estimates could be off (too large) by a factor of 2. *Abraham et al*. [2000] estimated values 0.5–5 $\mathrm{m^2\ s^{-1}}$ based on analysis of a phytoplankton bloom, implying factors of 1.7–2.7. It remains to be seen, however, whether the $\kappa^{-0.2}$ does hold down to very small κ, or whether, at some point, K_{OC} truly does become independent of κ. We speculate that higher resolution would lead to even less sensitivity to the value of κ, as observed for K_{eff} by *Marshall et al*. [2006].

Table B1. Average Numerical Diffusivity κ_{num} Diagnosed From (B1)

κ ($\mathrm{m^2\ s^{-1}}$)	κ_{num} ($\mathrm{m^2\ s^{-1}}$)
25	63 ± 12
50	83 ± 15
75	104 ± 17
100	126 ± 20
125	148 ± 23
150	171 ± 25

Appendix C: Variance Budgets

[63] It is edifying to explicitly calculate the variance budgets from our numerical simulations in order to better understand the assumptions underlying K_{OC}. We first examine the variance budget in the Pacific channel experiments. The zonal symmetry simplifies the budget and also facilitates easy comparison with of K_{OC} with K_{eff}. In a zonal average, indicated by the symbol $\bar{()}^x$, the variance budget (8) simplifies to

$$\frac{\partial}{\partial t}\frac{\bar{q}^{x}}{2} + \frac{\partial}{\partial y}\left(\frac{\overline{v'q'^2}^{x}}{2}\right) + \overline{v'q'}^{x}\frac{\partial\bar{q}^{x}}{\partial y} = \frac{\partial^2}{\partial y^2}\left(\kappa\frac{\overline{q'^2}^{x}}{2}\right) - \kappa\overline{|\nabla q'|^2}^{x}. \tag{C1}$$

[64] Because there is no mean meridional flow, the variance advection term only includes the triple correlation. The terms were diagnosed from the simulations and are shown as functions of y in Figure C1. The variance diffusion term (the first term on the right side of (C1)) was two orders of magnitude smaller than the others and so was not plotted. We did not diagnose the tendency term but instead assume it to be given by the residual. The dominant balance is clearly between variance production ($\overline{v'q'}^{x}\frac{\partial\bar{q}^{x}}{\partial y}$) which is everywhere

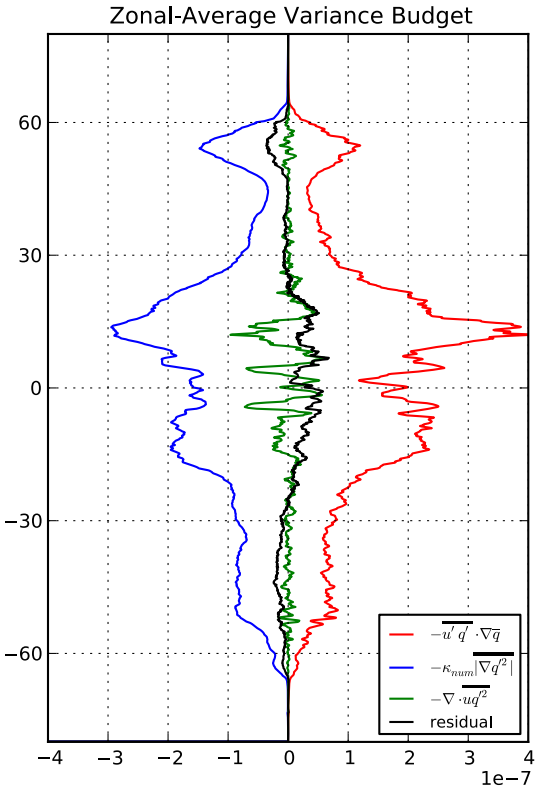

Figure C1. Terms in the zonal mean variance budget (C1). The tendency term was not diagnosed explicitly but is assumed to be equal to the residual.

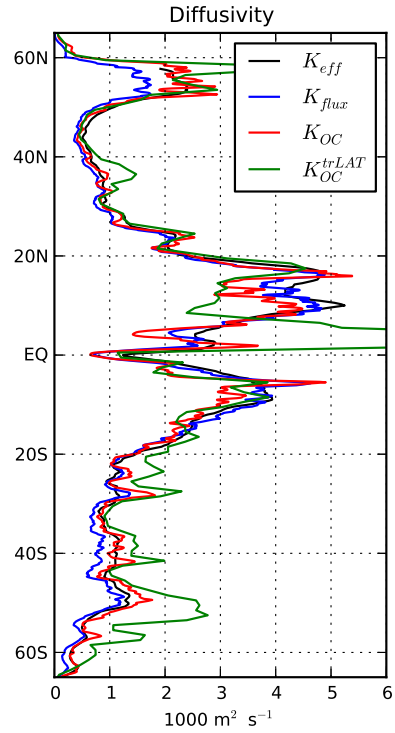

Figure C2. Comparison of three different diffusivity diagnostics (K_{eff}, K_{flux}, and K_{OC}) in the Pacific channel experiment. We also show the value of K_{OC} from the global `trLAT` experiment averaged over the same domain (the peak of this final quantity near the equator is not shown on the graph but reaches a maximum of close to 20,000 $\mathrm{m^2\ s^{-1}}$).

positive and variance destruction ($\kappa|\overline{\nabla q'}|^{2x}$), which is negative. The triple correlation term is generally much smaller. In some narrow peaks, its magnitude approaches 1/2 of the other two terms; however, positive peaks are neighbored by negative peaks, indicating that the term acts only to move variance around on small scales. The residual term is small, at maximum accounting for 20% of the balance. But the fact that it is nonzero indicates that the variance is not in a steady state, but rather is evolving slowly over the course of the year.

[65] Next, we consider the mixing diagnostic K_{OC} and compare it to K_{eff}. In a zonally averaged context, $K_{\mathrm{OC}} = \kappa|\overline{\nabla q'}|^{2x}/|\nabla\bar{q}^x|^2$. The third quantity worth comparing is

$$K_{\mathrm{flux}} = -\overline{v'q'}^x / \frac{\partial \bar{q}^x}{\partial y} \tag{C2}$$

a conventional diagnostic of mixing in channel flows. Based on our preceding discussion of the variance budget, we can see that K_{flux} is a diffusivity for the full cross-gradient flux, including the nonlocal part. Thus, we expect it to depart from K_{OC} wherever the tendency term or the triple correlation term is significant.

[66] We plot K_{eff}, K_{flux}, and K_{OC} in Figure C2; the agreement is quite good in most places. The slight disagreement between K_{flux} and K_{OC} near 55°N is easily attributed to the presence of a variance tendency at this latitude, apparent in Figure C1 (the same comment applies to the area around 40°S). Some disagreement between diagnostics is also evident in the peaks near the equator. The relatively strong

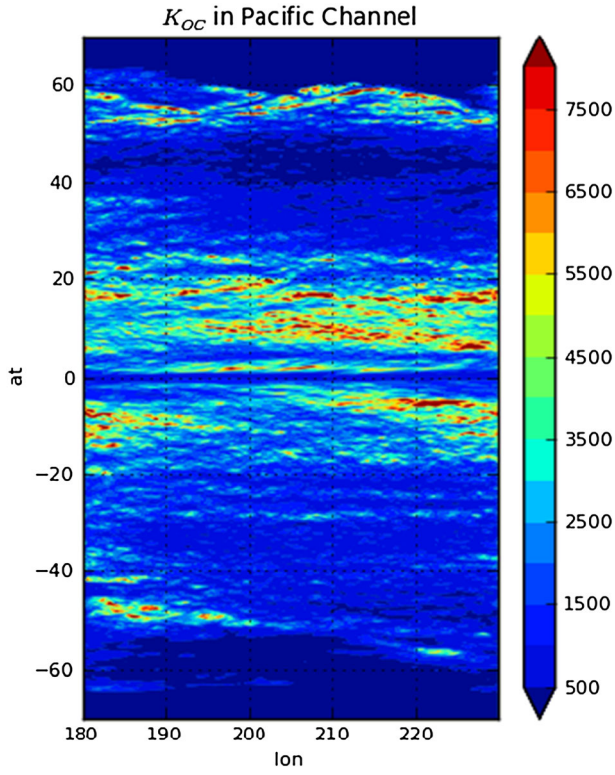

Figure C3. K_{OC} (11) computed locally in the Pacific channel experiment.

triple correlation term is likely responsible for this. Also, we note that in these regions, we found slight disagreement between K_{eff} obtained with different values of κ; we speculated that this could be due to spatially varying κ_{num} in regions of intense mixing. Overall though, these issues are small, and the three diagnostics give essentially the same results.

[67] We have also plotted K_{OC} from the global `trLAT` experiment in Figure C2 to facilitate a direct comparison between the global and sector results. Overall, the agreement is quite good; the primary difference is that the peak values in the global experiment are higher. This is due to much higher overall variance in the global experiment.

[68] The advantage of K_{OC} is that, unlike the other diagnostics, it can give a two-dimensional picture of mixing, revealing variation in x as well as y. To illustrate this, we simply compute the local value of K_{OC}, as defined in (11) (the zonal average of this quantity is identical to what is plotted in Figure C2). The full $K_{\mathrm{OC}}(x,y)$ is plotted in Figure C3. A high degree of zonal symmetry is indeed evident, but some zonal variations also emerge, for instance, between 20°S and the equator or near 50°S.

[69] Finally, we examine the full variance budget of (8) from our global experiments. Figures C4 and C5 show the relevant terms in the two-dimensional variance budget (8) for `trLAT` and `trPSI` (the variance budget for `trSST` is very similar to `trLAT` and is not plotted). Also plotted are the mean tracer concentration $\bar{q}$ and variance $\overline{q'^2}/2$. It is striking how different the variance field is for the different tracers. For `trPSI`, the region of highest variance is along the equator. This is due to the very strong background gradients of $\bar{q}$ which are present near the equator; these gradients in streamfunction coincide with the strong quasi-zonal equatorial jets. In contrast, the variance produced by `trLAT` is highest in boundary current regions.

[70] The variance budgets themselves reflect these differences. The variance production and dissipation for `trPSI` are both strongest at the equator, where the variance is highest. Likewise, these terms are most intense in the boundary currents for `trLAT`. As we saw in the zonally averaged budget (Figure C1), production is largely balanced locally by dissipation for both cases. The variance advection

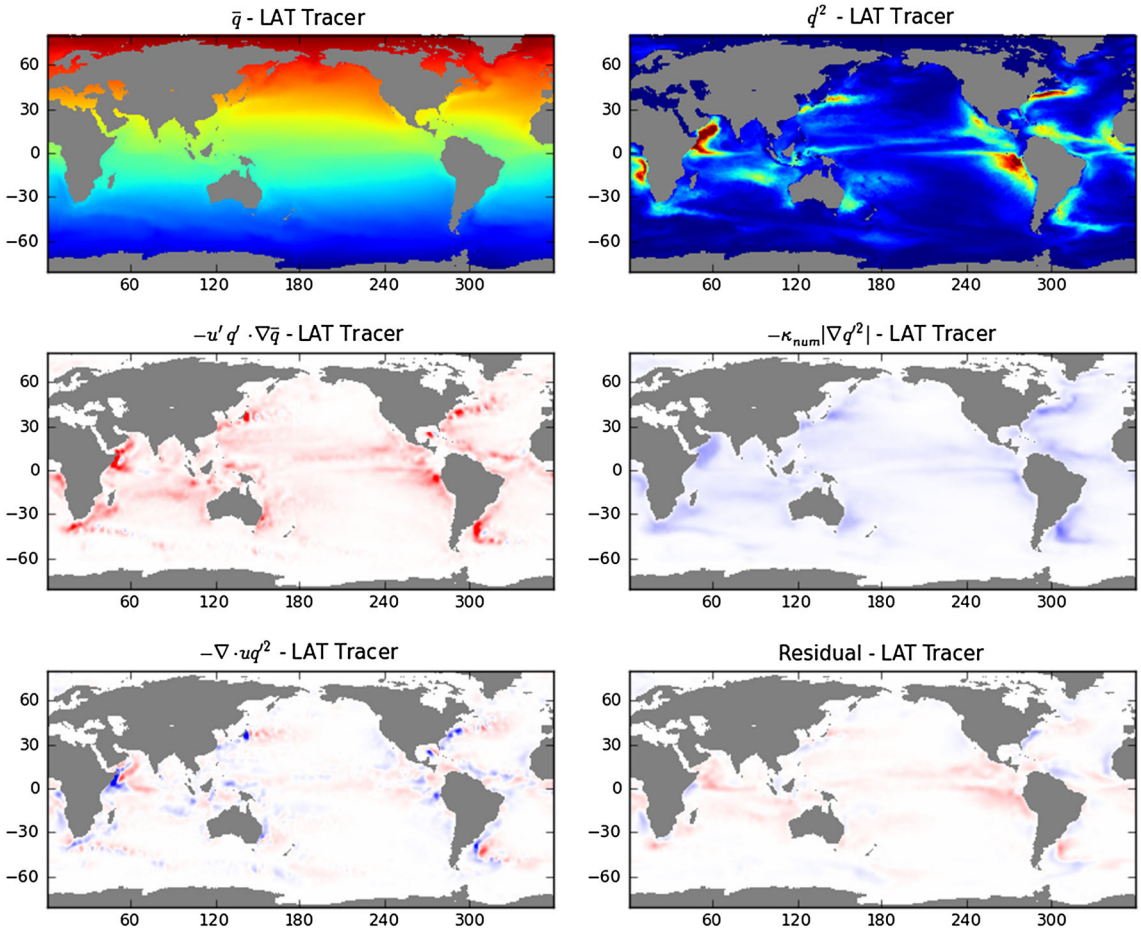

Figure C4. Diagnostics of tracer variance from the global `trLAT` experiments. The top row shows the mean tracer concentration $\bar{q}$ and variance $\overline{q'^2}/2$. The magnitude of the terms is meaningless, since the tracer units themselves are arbitrary. In the bottom four panels, the terms of the variance budget (8) are all arranged on the right side of the equation, so that a positive value acts to locally increase the variance (the bottom four panels are plotted with the same color scale, with red indicating positive and blue negative. The residual, shown in the bottom right panel, is assumed to correspond to a net tendency (the tendency was not diagnosed explicitly).

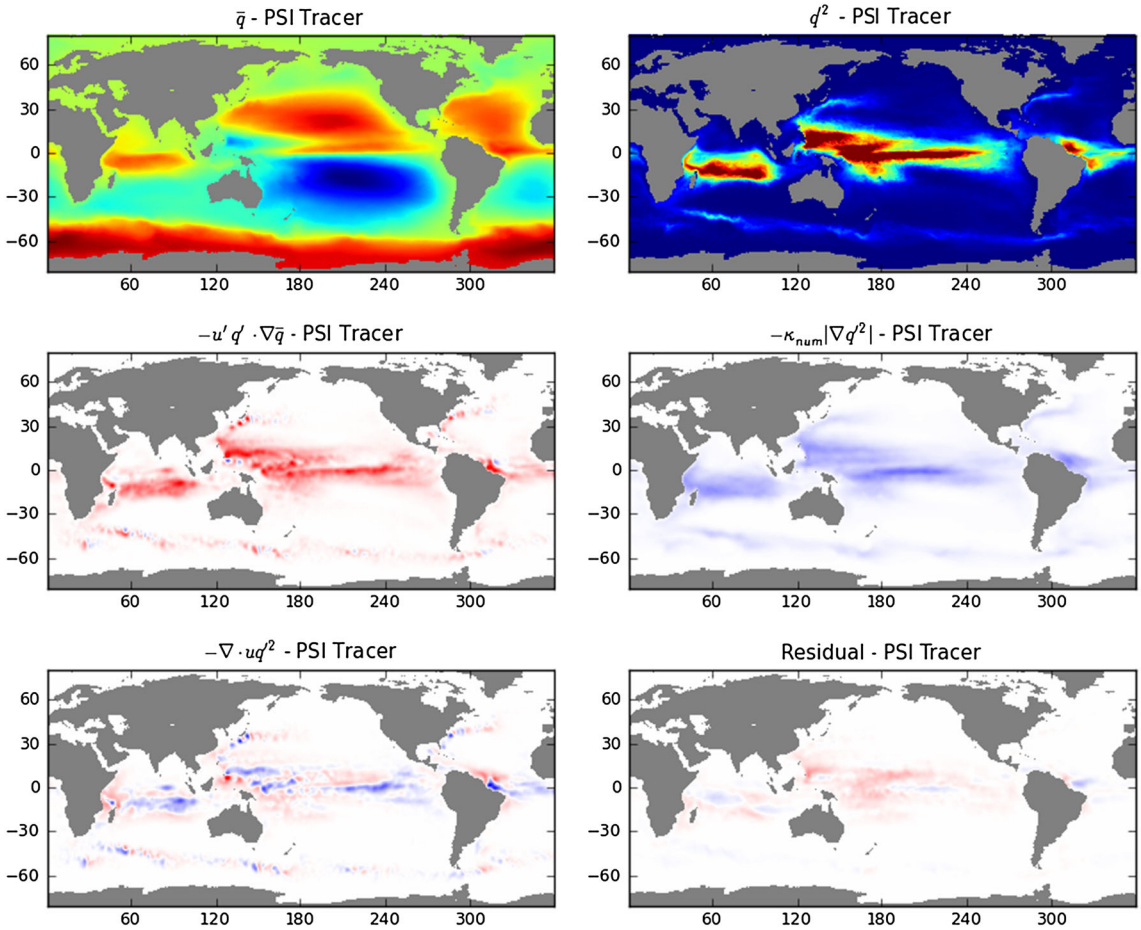

Figure C5. Same as Figure C4 but for `trPSI`.

(which includes both triple correlation and mean advection) mostly displays intense small-scale variations on scales below 500 km, with closely neighboring sites of positive and negative contributions. This means that variance is generally dissipated within 500 km, or less, of where it is produced, implying that *on large scales*, the variance budget is approximately local. The areas where the advection terms are significant are mostly in boundary currents, the ACC, or near the equator.

[71] The only glaring exception to this quasi-local balance is in near the equator for `trPSI`, where coherent zonal bands of positive and negative values are present. These bands indicate a systematic transfer of variance from a production region to a dissipation region. We note that this transfer is truly a combination of triple correlation and mean variance advection, rather than being due just to one term, although only the net advection is plotted.

[72] **Acknowledgments.** We thank Raf Ferrari, David Ferreira, Andreas Klocker, Alan Plumb, and Ross Tulloch for helpful discussions. We also thank three anonymous reviewers. The altimeter products were produced by Ssalto/Duacs and distributed by AVISO, with support from Cnes (http://www.aviso.oceanobs.com/duacs/). The authors also acknowledge support from NSF through the MOBY project, an MIT, WHOI, NCAR collaboration which explores the role of eddies in ocean circulation.

References

Abernathey, R., J. Marshall, E. Shuckburgh, and M. Mazloff (2010), Enhancement of mesoscale eddy stirring at steering levels in the southern ocean, *J. Phys. Oceanogr.*, *40*, 170–185.

Abraham, E. R., C. S. Law, P. W. Boyd, S. J. Lavender, and M. T. Maldonado (2000), Importance of stirring in the development of an iron-fertilized phytoplankton bloom, *Nature*, *407*, 727–730.

Bennet, A. F. (1984), Relative dispersion: Local and nonlocal dynamics, *J. Atmos. Sci.*, *41*, 1881–1886.

Bower, A. S., H. T. Rossby, and J. L. Lillibridge (1985), The gulf stream–barrier or blender, *J. Phys. Oceanogr.*, *15*, 24–33.

Chelton, D. B., and M. G. Schlax (1996), Global observations of oceanic Rossby waves, *Science*, *272*(5259), 234–238.

Chelton, D. B., M. G. Schlax, and R. M. Samelson (2011), Global observations of nonlinear mesoscale eddies, *Prog. Oceanogr.*, *91*, 167–216.

Danabasoglu, G., and J. C. McWilliams (1995), Sensitivity of the global ocean circulation to parameterizations of mesoscale tracer transports, *J. Clim.*, *8*, 2967–2987.

Davis, R. (1991), Observing the general circulation with floats, *Deep Sea Res.*, *38A*, S531–S571.

de Szoeke, R. A., and M. D. Levine (1981), The advective flux of heat by mean geostrophic motions in the southern ocean, *Deep Sea Res.*, *28A* (10), 1057–1085.

Ferrari, R., and M. Nikurashin (2010), Suppression of eddy diffusivity across jets in the southern ocean, *J. Phys. Oceanogr.*, *40*.

Fox-Kemper, B., R. Lumpkin, and F. O. Bryan (2012), Lateral transport in the ocean interior, in *Ocean Circulation and Climate – Observing and Modelling the Global Ocean*, edited by G. Siedler, J. Church, J. Gould, and S. Griffies, Elsevier. Submitted.

Gent, P., and J. McWilliams (1990), Isopycnal mixing in ocean circulation models, *J. Phys. Oceanogr.*, *20*, 150–155.

Gill, A. E., J. S. A. Green, and A. J. Simmons (1974), Energy partition in the large-scale ocean circulation and the production of mid-ocean eddies, *J. Marine Res.*, *21*, 499–528.

Green, J. S. A. (1970), Transfer properties of the large-scale eddies and the general circulation of the atmosphere, *Quart. J. Roy. Meteor. Soc.*, *96*, 157–185.

Griesel, A., S. Gille, J. Sprintall, J. L. McClean, J. H. Lacasce, and M. E. Maltrud (2010), Isopycnal diffusivities in the Antarctic Circumpolar Current inferred from Lagrangian floats in an eddying model, *J. Geophys. Res.*, *115*, C06,006, in Preparation.

Griffies, S. M. (1998), The Gent-McWilliams skew flux, *J. Phys. Oceanogr.*, *28*, 831–841.

Haynes, P., and E. Shuckburgh (2000a), Effective diffusivity as a diagnostic of atmospheric transport. Part i: Stratosphere, *J. Geophys. Res.*, *105*, 22,777–22,794.

Haynes, P., and E. Shuckburgh (2000b), Effective diffusivity as a diagnostic of atmospheric transport. Part ii: Troposphere and lower stratosphere, *J. Geophys. Res.*, *105*, 795–810.

Hill, C., D. Ferreira, J.-M. Campin, J. Marshall, R. Abernathey, and N. Barrier (2012), Controlling spurious diapycnal mixing in eddy-resolving height-coordinate ocean models: Insights from virtual deliberate tracer release experiments, *Ocean Model.*, *45–46*, 14–26.

Holloway, G. (1986), Estimation of oceanic eddy transports from satellite altimetry, *Nature*, *323*, 343–344.

Johnson, G. C., and H. L. Bryden (1989), On the size of the Antarctic Circumpolar Current, *Deep Sea Res.*, *36*, 39–53.

Kamenkovich, I., I. P. Berloff, and J. Pedlosky (2009), Anisotropic material transport by eddies and eddy-driven currents in a model of the north Atlantic, *J. Phys. Oceanogr.*, *39*, 3162–3175, doi:10.1175/2009JPO4239.1.

Keffer, T., and G. Holloway (1988), Estimating southern ocean eddy flux of heat and salt from satellite altimetry, *Nature*, *332*, 624–626.

Klocker, A., R. Ferrari, and J. H. LaCasce (2012a), Estimating suppression of eddy mixing by mean flow, *J. Phys. Oceanogr.*, *42*, 1566–1576.

Klocker, A., R. Ferrari, J. H. LaCasce, and S. T. Merrifield (2012b), Reconciling float-based and tracer-based estimates of eddy diffusivities, *J. Marine Res.*, in press.

Koszalka, I., J. H. LaCasce, and K. A. Orvik (2009), Relative dispersion in the Nordic seas, *J. Marine Res.*, *67*, 411–433.

LaCasce, J. H. (2008), Statistics from Lagrangian observations, *Prog. Oceanogr.*, *77*, 1–29.

LaCasce, J. H., and A. Bower (2000), Relative dispersion in the subsurface north Atlantic, *J. Marine Res.*, *58*, 863–894.

LaCasce, J. H., and C. Ohlmann (2003), Relative dispersion at the surface of the Gulf of Mexico, *J. Marine Res.*, *61*(3), 285–312.

Lagerloef, G., G. Mitchum, R. Lukas, and P. Niiler (1999), Tropical Pacific near-surface currents estimated from altimeter, wind and drifter data, *J. Geophys. Res.*, *104*, 313–23.

Lapeyre, G. (2009), What vertical mode does the altimeter reflect? On the decomposition in baroclinic modes and on a surface-trapped mode, *J. Phys. Oceanogr.*, *39*, 2857–2874.

Ledwell, J. R., A. J. Watson, and C. S. Law (1998), Mixing of a tracer in the pycnocline, *J. Geophys. Res.*, *103*(C10), 21,499–21,592.

Liu, C., A. Köhl, and D. Stammer (2012), Adjoint based estimation of eddy induced tracer mixing parameters in the global ocean, *J. Phys. Oceanogr.*, *42*, 1186–1206.

Lu, J., and K. Speer (2010), Topography, jets, and eddy mixing in the southern ocean, *J. Marine Res.*, *68*, 479–502.

Lumpkin, R., and S. Elipot (2010), Surface drifter pair spreading in the north Atlantic, *J. Geophys. Res.*, *115*, C12,017.

Lumpkin, R., A. M. Treguier, and K. Speer (2002), Lagrangian eddy scales in the northern Atlantic ocean, *J. Phys. Oceanogr.*, *32*, 2425–2440.

Marshall, J., and G. Shutts (1981), A note on rotational and divergent eddy fluxes, *J. Phys. Oceanogr.*, *21*, 1677–1681.

Marshall, J., A. Adcroft, C. Hill, L. Perelman, and C. Heisey (1997a), A finite-volume, incompressible Navier Stokes model for studies of the ocean on parallel computers, *J. Geophys. Res.*, *102*, 5753–5766.

Marshall, J., C. Hill, L. Perelman, and A. Adcroft (1997b), Hydrostatic, quasi-hystrostatic, and non-hydrostatic ocean modeling, *J. Geophys. Res.*, *102*, 5733–5752.

Marshall, J., E. Shuckburgh, H. Jones, and C. Hill (2006), Estimates and implications of surface eddy diffusivity in the southern ocean derived from tracer transport, *J. Phys. Oceanogr.*, *36*, 1806–1821.

Nakamura, N. (1996), Two-dimensional mixing, edge formation, and permeability diagnosed in an area coordinate, *J. Atmos. Sci.*, *53*, 1524–1537.

Nakamura, N. (2001), A new look at eddy diffusivity as a mixing diagnostic, *J. Atmos. Sci.*, *58*, 3685–3702.

Nakamura, N. (2008), Quantifying inhomogeneous, instantaneous, irreversible transport using passive tracer field as a coordinate, *Lect. Notes Phys.*, *744*, 137–164.

Nakamura, N., and J. Ma (1997), Modified Lagrangian-mean diagnostics of the stratospheric polar vortices 2. nitrous oxide and seasonal barrier migration in the cryogenic limb array etalon spectrometer and SKYHI general circulation model, *J. Geophys. Res.*, *102*, 25,721–25,735.

Orsi, A. H., T. W. Whitworth, and W. D. Nowlin (1995), On the meridional extent and fronts of the Antarctic Circumpolar Current, *Deep Sea Res I*, *42*(5), 641–673.

Osborn, T. R., and C. S. Cox (1972), Oceanic fine structure, *Geol. Astron. Fluid Dyn.*, *3*(1), 321–345.

Ottino, J. M. (1989), *The Kinematics of Mixing: Stretching, Chaos, and Transport*, Cambridge University Press, Cambridge.

Owens, W. B. (1984), A synoptic and statistical description of the gulf stream and subtropical gyre using SOFAR floats, *J. Phys. Oceanogr.*, *14*, 104–113.

Picaut, J., S. P. Hayes, and M. J. McPhaden (1989), Use of the geostrophic approximation to estimate time-varying zonal currents at the equator, *J. Geophys. Res.*, *94*(C3), 3228–3236.

Plumb, R. A. (1979), Eddy fluxes of conserved quantities by small-amplitude waves, *J. Atmos. Sci.*, *36*, 1699–1705.

Plumb, R. A., and J. D. Mahlman (1987), The zonally-averaged transport characteristics of the GFDL general circulation/tracer model, *J. Atmos. Sci.*, *44*, 298–327.

Prandtl, L. (1925), Bericht untersuchungen zur ausgebildeten turbulenz, *Zs. Angew. Math. Mech.*, *5*, 136–139.

Redi, M. (1982), Oceanic isopycnal mixing by coordinate rotation, *J. Phys. Oceanogr.*, *12*, 1154–1158.

Richardson, L. F. (1926), Atmospheric diffusion on a distance-neighbor graph, *Proc. R. Soc. London A*, *110*, 707–737.

Roe, P. (1985), Some contributions to the modelling of discontinuous flows, *Large-scale Comput. Fluid Mech.*, *1*, 163–193.

Rypina, I. I., I. Kamenkovich, P. Berloff, and L. Pratt (2012), Eddy-induced particle dispersion in the near-surface, *J. Phys. Oceanogr.*

Sallée, J. B., K. Speer, R. Morrow, and R. Lumpkin (2008), An estimate of Lagrangian eddy statistics and diffusion in the mixed layer of the southern ocean, *J. Marine Res.*, *66*(4), 441–463.

Scott, R. B., and D. G. Furnival (2012), Assessment of traditional and new eigenfunction bases applied to extrapolation of surface geostrophic current time series to below the surface in an idealized primitive equation simulation, *J. Phys. Oceanogr.*, *42*, 165–178.

Shuckburgh, E., and P. Haynes (2003), Diagnosing transport and mixing using a tracer-based coordinate system, *Physics of Fluids*, *15*(11), 3342–3357.

Shuckburgh, E., H. Jones, J. Marshall, and C. Hill (2009a), Robustness of effective diffusivity diagnostic in oceanic flow, *J. Phys. Oceanogr.*, *39*, 1993–2009, in Press.

Shuckburgh, E., H. Jones, J. Marshall, and C. Hill (2009b), Understanding the regional variability of eddy diffusivity in the pacific sector of the southern ocean, *J. Phys. Oceanogr.*, *39*, 2011–2023, in Press.

Smith, K. S., and J. Marshall, Evidence for enhanced eddy mixing at mid-depth in the southern ocean, *J. Phys. Oceanogr.*, *39*, 50–69, 2009.

Stammer, D. (1998), On eddy characteristics, eddy transports, and mean flow properties, *J. Phys. Oceanogr.*, *28*, 727–739.

Taylor, G. I. (1921), Diffusion by continuous movements, *Proc. London Math. Soc.*, *s2-20*, 196–212.

Tulloch, R., J. Marshall, and K. S. Smith (2009), Interpretation of the propagation of surface altimetric observations in terms of planetary waves and geostrophic turbulence, *J. Geophys. Res.*, *114*, C02,005.

Waugh, D. W., and E. R. Abraham (2008), Stirring in the global surface ocean, *Geophys. Res. Lett.*, *35*, L20,605.

Wilson, C., and R. G. Williams (2004), Why are eddy fluxes of potential vorticity difficult to parameterize?, *J. Phys. Oceanogr.*, *34*, 142–155.

Winters, K., and E. D'Asaro (1996), Diascalar flux and the rate of fluid mixing, *J. Fluid Mech.*, *317*, 179–193.

Wunsch, C. (1997), The vertical partition of oceanic horizontal kinetic energy and the spectrum of global variability, *J. Phys. Oceanogr.*, *27*, 1770–1794.

Wunsch, C., and R. Ferrari (2004), Vertical mixing, energy, and the general circulation of the ocean, *Annu. Rev. Fluid Mech.*, *36*, 281–314.

Wunsch, C., and P. Heimbach (2009), The globally integrated ocean circulation (MOC), 1992–2006: Seasonal and decadal variability, *J. Phys. Oceanogr.*, *39*(2), 351–368.

Young, W. R., P. B. Rhines, and C. J. R. Garrett (1982), Shear-flow dispersion, internal waves and horizontal mixing in the ocean, *J. Phys. Oceanogr.*, *12*, 515–527.

Zhurbas, V., and I. S. Oh (2003), Lateral diffusivity and Lagrangian scales in the Pacific ocean as derived from drifter data, *J. Geophys. Res.*, *108* (C5), 3141.

Zhurbas, V., and I. S. Oh (2004), Drifter-derived maps of lateral diffusivity in the Pacific and Atlantic oceans in relation to surface circulation patterns, *J. Geophys. Res.*, *109*, C05,015.